NaDyF4 Nanoparticles as T−2 Contrast Agents for Ultrahigh Field Magnetic Resonance Imaging

ARTICLE *in* JOURNAL OF PHYSICAL CHEMISTRY LETTERS · FEBRUARY 2012

Impact Factor: 7.46 · DOI: 10.1021/jz201664h

7 AUTHORS, INCLUDING:

Gautom K Das
Rice University
23 PUBLICATIONS **485** CITATIONS
SEE PROFILE

Noah J J Johnson
University of California, San Diego
17 PUBLICATIONS **592** CITATIONS
SEE PROFILE

THE JOURNAL OF PHYSICAL CHEMISTRY Letters

Letter

pubs.acs.org/JPCL

$NaDyF_4$ Nanoparticles as T_2 Contrast Agents for Ultrahigh Field Magnetic Resonance Imaging

Gautom Kumar Das,[†] Noah J. J. Johnson,[†] Jordan Cramen,[†] Barbara Blasiak,[‡] Peter Latta,[‡] Boguslaw Tomanek,[‡] and Frank C. J. M. van Veggel*,[†]

[†]Department of Chemistry, University of Victoria, P.O. Box 3065, Victoria, British Columbia, Canada V8W 3V6

[‡]Institute for Biodiagnostics (West), National Research Council of Canada, Calgary, Alberta, Canada T2N 4N1

Supporting Information

ABSTRACT: A major limitation of the commonly used clinical MRI contrast agents (CAs) suitable at lower magnetic field strengths (<3.0 T) is their inefficiency at higher fields (>7 T), where next-generation MRI scanners are going. We present dysprosium nanoparticles (β-$NaDyF_4$ NPs) as T_2 CAs suitable at ultrahigh fields (9.4 T). These NPs effectively enhance T_2 contrast at 9.4 T, which is 10-fold higher than the clinically used T_2 CA (Resovist). Evaluation of the relaxivities at 3 and 9.4 T show that the T_2 contrast enhances with an increase in NP size and field strength. Specifically, the transverse relaxivity (r_2) values at 9.4 T were ~64 times higher per NP (20.3 nm) and ~6 times higher per Dy^{3+} ion compared to that at 3 T, which is attributed to the Curie spin relaxation mechanism. These results and confirming phantom MR images demonstrate their effectiveness as T_2 CAs in ultrahigh field MRIs.

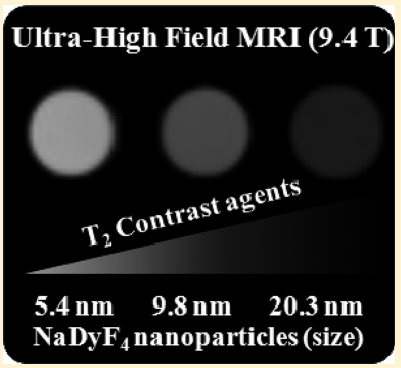

SECTION: Nanoparticles and Nanostructures

Magnetic resonance imaging (MRI), one of the most powerful noninvasive imaging techniques in diagnostic radiology, has been shifting toward higher magnetic fields (>3 T) to achieve a higher signal-to-noise ratio and thus greater spatial and temporal resolution.[1−4] Furthermore, preclinical MRI studies with small animal models must provide the highest possible resolution; hence they rely heavily on very high field strengths (>7 T). The contrast-to-noise ratio in MRI is often improved by using contrast agents (CAs), which selectively shorten the T_1 or T_2 relaxation times in the region of interest, providing enhancement of pathology.[5−7] The efficiency of a CA depends on its r_1 ($1/T_1$) and r_2 ($1/T_2$) relaxivity as well as the r_2/r_1 ratio. The higher the ratio of r_2/r_1, the better the efficiency of a T_2 CA and vice versa for a T_1 CA.[8,9] One of the major limitations of the present clinically used CAs is their decreased efficiency at higher magnetic fields. For example, Gd^{3+} complexes, the widely used T_1 CAs, are optimal at fields below 1 T; even at clinical field strength (3 T), the T_1 relaxivity of Gd^{3+}-based CAs is reduced by as much as one-third compared to its maximum.[2,10−12] The other type of clinically used CAs (i.e., superparamagnetic iron oxide (SPIO) nanoparticles for T_2 contrast) are known to saturate their magnetization at around 1.5 T, which limits their MR efficiency at high magnetic fields.[11] Therefore, development of CAs efficient at high magnetic field becomes an urgent task to take full advantage of contrast-enhanced MR imaging at ultrahigh fields, so as to meet the ever-growing performance demand as emphasized in recent reviews.[12,13]

The paramagnetic dysprosium (Dy^{3+}) ion has been proposed as one of the best choices for T_2 CA at high field MRI because of its high magnetic moment (10.6 μ_B) and short electronic relaxation time (~0.5 ps).[12,13] However, until now, only a handful of Dy^{3+}-based chelates (e.g., Dy^{3+}-DTPA) and NPs (e.g., Dy_2O_3) have been studied as T_2 CAs.[14−20] In general, NP-based CAs offer more advantages than the respective chelates. NPs have the freedom of precise size and shape tuning with ease of surface functionalization for prolonged blood circulation, selective targeting, and therapy. Furthermore, NPs contain a high load of paramagnetic ions per volume, enabling local contrast enhancement, which is many times higher than that provided by the chelates. In addition, both monodispersity and uniformity of the NPs are extremely important for homogeneous biodistribution, clearance from the body, as well as maintaining consistent properties. Most importantly, in vivo applications require a hydrodynamic diameter (HD) of a NP to be below 50 nm to allow long circulation time and to avoid nonspecific uptake.[21] Yet, no studies have been reported elucidating the potential of Dy^{3+}-based uniform, monodisperse NPs with HD below 50 nm that have investigated their relaxivity at higher magnetic fields. The oxide-based NPs (Dy_2O_3 and rare earth (RE) oxides, in general) explored thus far still have not achieved the precise size control and tunability that is available with fluoride-based ($NaREF_4$) NPs.

Received: December 19, 2011
Accepted: February 3, 2012

   dx.doi.org/10.1021/jz201664h | J. Phys. Chem. Lett. 2012, 3, 524−529

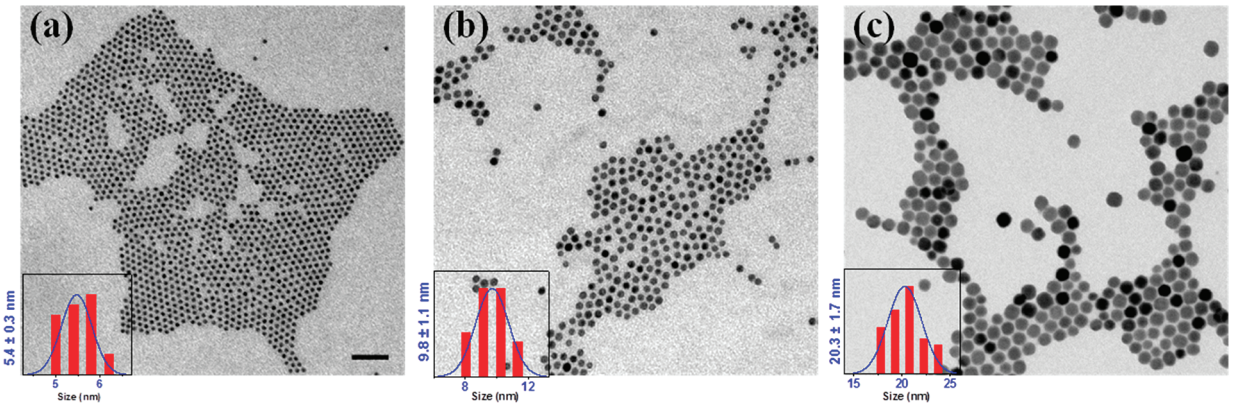

Figure 1. TEM images of the synthesized β-$NaDyF_4$ NPs, (a) 5.4 ± 0.3, (b) 9.8 ± 1.1, and (c) 20.3 ± 1.7 nm. The inset shows the size analysis of the nanoparticles of at least 50 nanoparticles in each histogram. The scale bar is 50 nm for all three images.

In this work, we report relaxivity of dysprosium (at 3 and 9.4 T) with synthetically controlled β-$NaDyF_4$ NPs in the range of ∼5−20 nm, with associated nanoscale tunability in terms of size, magnetism, and induced magnetic nuclear spin relaxation. The NPs were tuned to ∼5−20 nm (with HD as high as 33.7 nm) due to their superior biocompatibility within this size regime while keeping the size of the NPs similar to the clinically used SPIO-based T_2 CAs.[5−7]

A high-temperature synthesis has been used to grow the β-$NaDyF_4$ NPs in a binary mixture of octadecene and oleic acid (see the experimental section in the Supporting Information). By controlling the nucleation and growth phase of the nanocrystal, uniform NPs have been grown.[22] Synthesis conditions are summarized in Table S1 (Supporting Information). Transmission electron microscopy (TEM) images of the β-$NaDyF_4$ NPs show uniform and monodisperse 5.4 ± 0.3, 9.8 ± 1.1, and 20.3 ± 1.7 nm NPs (Figure 1). Powder X-ray diffraction (XRD) patterns (Figure S1, Supporting Information) confirm the hexagonal phase of $NaDyF_4$ NPs (PDF# 00-027-0687), while size analyses using Scherrer's equation were found to be in good agreement with the sizes measured with TEM (Table S1, Supporting Information). The broadening of the XRD peaks is further evidence of the small crystallite size of the NPs, with peaks sharpening toward the larger sizes. Our synthesis technique allowing size control of monodisperse NPs (by careful control of the amount of coordinating oleic acid) can be extended to the synthesis of other lanthanide tetrafluoride NPs, where tunability in this size regime is required for MRI and other applications.[23−29]

The as-synthesized NPs were coated with hydrophobic oleate ligands and thus were not dispersible in water. An intercalation strategy has been employed to render them water-dispersible using an amphiphilic polymer, that is, poly(maleic anhydride-*alt*-1-octadecene)-polyethylene glycol (PMAO-PEG). Characterization details of the PMAO-PEG and a schematic representation of the phase transfer strategy are presented in Figure S2, Supporting Information. The TEM images of NPs after intercalation show that they are well-separated and thus form stable dispersions without any discernible aggregation even after 12 weeks of storage (Figure S3, Supporting Information). The intercalated NPs were further characterized by dynamic light scattering (DLS) to measure the HD of the NPs in water dispersion. The HD is important in determining the rotational correlation time of the NPs, which influences relaxivity. The measured HDs of the NPs were between ∼18 to 33 nm (Table S1, Supporting Information) for the three different sizes of NPs, suggesting that the NPs are covered with a ∼7 nm thick organic layer.

The MR relaxivity of these NP-based CAs was investigated at 3 and 9.4 T to observe their effects at clinical and ultrahigh magnetic fields, respectively. We observed that (i) the r_2 relaxivities of the NPs are very much pronounced compared to r_1 relaxivities for all three sizes of the β-$NaDyF_4$ NPs at both magnetic fields and (ii) the r_2 relaxivities increase with larger NPs, and the enhancement can be as high as ∼9 fold at 9.4 T compared to the relaxivity at 3 T.

In principle, the enhanced T_2 relaxation is observed due to the field perturbation caused by the magnetic susceptibility of the CAs. Dy^{3+}, being highly susceptible due to its large magnetic moment (μ_S), shows higher impact on the r_2 relaxivity than on the r_1 relaxivity at any field strength (Figure 2). The short electronic relaxation time of Dy^{3+} (τ_e = 0.5 ps), which is due to the anisotropic ground state of Dy^{3+} ions, has greatly reduced their T_1 relaxation, which results in a flat line throughout the NP size range and field strengths (Figure 2a).[19] However, the magnitude of τ_e does not affect the susceptibility contribution of Dy^{3+} toward higher magnetic fields, which increases drastically with the field. The susceptibility contribution arises from the average alignment of Dy^{3+} magnetic moments along the applied field. Therefore, the obtained r_2 relaxivities are always higher than the r_1 relaxivity. The r_2 relaxivities of the NPs obtained at 9.4 and 3 T are summarized in terms of ionic, mass, and per-NP-based relaxivity in Table 1 and Table S2 (Supporting Information).

Larger β-$NaDyF_4$ NPs show higher relaxivity compared to the small ones. This is primarily ascribed to the higher magnetization of big NPs than the smaller ones.[30] The magnetization plots (M−H) obtained for the β-$NaDyF_4$ NPs show that the NPs are paramagnetic, with magnetization values of 6.53, 8.09, 8.97 emu/g for the 5.4, 9.8, and 20.3 nm NPs, respectively, at 50 KOe (Figure 3). The higher magnetization of big NPs can be explained by "spin-canting effects", which implies that with the decrease in the NPs size, the surface-to-volume ratio increases, and curvature of the NPs becomes more pronounced. As a result, spins located near the surface tend to be slightly tilted (i.e., canted spins) and result in a low magnetization value for the small NPs compared to that for the big ones.[30]

However, enhancement of the r_2 relaxivity is ∼6−9-fold at 9.4 T compared to that at 3 T. In principle, the relaxation rate enhancement induced by a paramagnetic lanthanide ion is the sum of the following four contributions, diamagnetic (R_{idia}),

dx.doi.org/10.1021/jz201664h | *J. Phys. Chem. Lett.* 2012, 3, 524−529

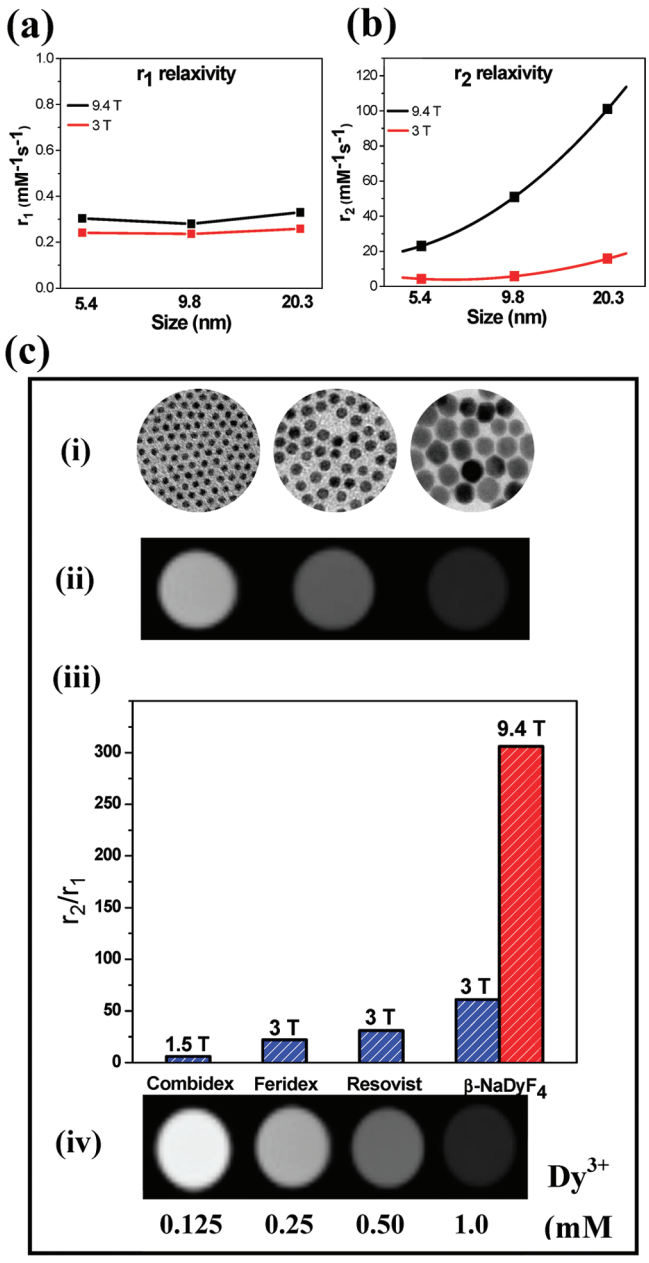

Figure 2. (a) Longitudinal (r_1) and (b) transverse (r_2) relaxivity obtained for the three sizes of β-$NaDyF_4$ NPs at 3 and 9.4 T. (c) (i) TEM representations of the 5.4, 9.8, 20.3 nm NPs, (ii) phantom images of the NPs from small to big (left to right) at a 1.0 mM Dy^{3+} ion concentration at 9.4 T, (iii) comparison of r_2/r_1 values among the commercial T_2 CAs and the 20.3 nm β-$NaDyF_4$ NPs, and (iv) concentration-dependent phantom image contrast of the 20.3 nm NPs at 9.4 T.

Table 1. Transverse Relaxivity (r_2) and the r_2/r_1 Ratio Obtained at 9.4 T for the β-$NaDyF_4$ NPs in Water[a]

size nm	$r_2[Dy^{3+}]$ mM^{-1} s^{-1}	$r_2[M]$ $(mg/mL)^{-1}$ s^{-1}	$r_2[NP]$ mM^{-1} s^{-1}	r_2/r_1
20.3	101	392	6479	306
9.8	51	200	350	230
5.4	32	125	50	106

[a] $r_2[Dy^{3+}]$: relaxivity per Dy^{3+} ion; $r_2[M]$: relaxivity per mass of β-$NaDyF_4$ NPs; $r_2[NP]$: relaxivity per β-$NaDyF_4$ NP.

dipolar (R_{iD}), contact (R_{iC}), and Curie ($R_{i\chi}$), and can be expressed as $R_i = R_{idia} + R_{iD} + R_{iC} + R_{i\chi}$ ($R_i = 1/T_i$; $i = 1, 2$). The diamagnetic contribution to the relaxivity is negligible for water protons, and contact contribution is much smaller than the dipolar and Curie terms for the lanthanides (except Gd^{3+}) and can thus be neglected.[19] Hence, dipolar and Curie components stand out for the relaxivity enhancement of the β-$NaDyF_4$ NPs. The dipolar effect is a spatial effect that is the result of the dipolar coupling between the spin of the unpaired electrons of the Dy^{3+} and nuclear spins of protons, which is a function of effective magnetic moment (μ_{eff}) of the Dy^{3+} ions and the following correlation times: τ_M (residence time of the coordinated water molecules before exchanging with bulk water molecules), τ_R (rotational correlation time), and τ_e (electronic relaxation time). The Curie component, on the other hand, depends on the square of applied magnetic field and the correlation times τ_R and τ_M. (see Supporting Information). Thus, for the same size NP, the Curie spin relaxation would be responsible for an increment of the relaxivity by a factor of 9.8 (as the field goes up from 3 to 9.4 T) if other parameters remain approximately constant. However, the τ_R is different for different size NPs. We calculated the approximate values of τ_R based on the Debye–Stokes equation (see Supporting Information), which suggests that the 20.3 nm NPs tumble at the slowest time of 4.38 μs compared to the 9.8 and 5.4 nm NPs (τ_R is 2.08 and 0.73 μs, respectively). However, considering the same polymer on the NP surface (i.e., PMAO-PEG), τ_M should not differ by more than an order of magnitude per Dy^{3+} ion of different NPs.[3] Due to the complex nature of the relaxivity equations, it is difficult to predict precisely the effect of the correlation times without accurate measurements. In any case, the obtained results suggest that the relaxivity enhancements are close to the factor of the square of the increment of the magnetic field. Taking into account the case of nanoparticles of Dy_2O_3 previously studied by Peters et al., the spatial variation of the local field inhomogeneities arising from a single particle is less pronounced for small nanoparticles, and the general expectation of increase in relaxivity to the square of the increment of the magnetic field is satisfied.[19,20] As explained in their report, this is satisfied for nanoparticles with diffusion correlation times of $\tau_D < 1.5 \times 10^{-6}$ s ($\tau_D = r_c^2/D$, where r_c is the core NP radius and $D = 2.5 \times 10^{-9}$ m^2 s^{-1} is the diffusion coefficient of water at 25 °C). For the β-$NaDyF_4$ NPs (20.3 nm) analyzed here, the diffusion correlation time τ_D is $\sim 4 \times 10^{-8}$ s. This is almost 2 orders of magnitude lower than the above criterion; hence, local field inhomogeneities should be negligible. The outer-sphere model then applies to describe the relaxivity. This outer-sphere model breaks down for sizes well above 50 nm and at field strengths > 12 T.[20] Therefore, it is reasonable that the Curie spin relaxation is the main mechanism responsible for the high enhancement of relaxivity at ultrahigh magnetic fields for the β-$NaDyF_4$ NPs in the size range of 5–20 nm. However, detailed studies, for example, with variable-temperature ^{17}O NMR spectroscopy, should be performed to estimate the residence time of the coordinated water molecules and to elucidate this mechanism with greater understanding. Notwithstanding the above, the trend of the big enhancement of the r_2 relaxivity of the β-$NaDyF_4$ NPs is in good agreement with the observed enhancement for Dy-DTPA complexes by Caravan et al. and other investigators.[11,31,32]

It is noteworthy to mention that the 20.3 nm β-$NaDyF_4$ NPs possess an extremely high r_2/r_1 ratio (i.e., 306) at 9.4 T. As

dx.doi.org/10.1021/jz201664h | J. Phys. Chem. Lett. 2012, 3, 524–529

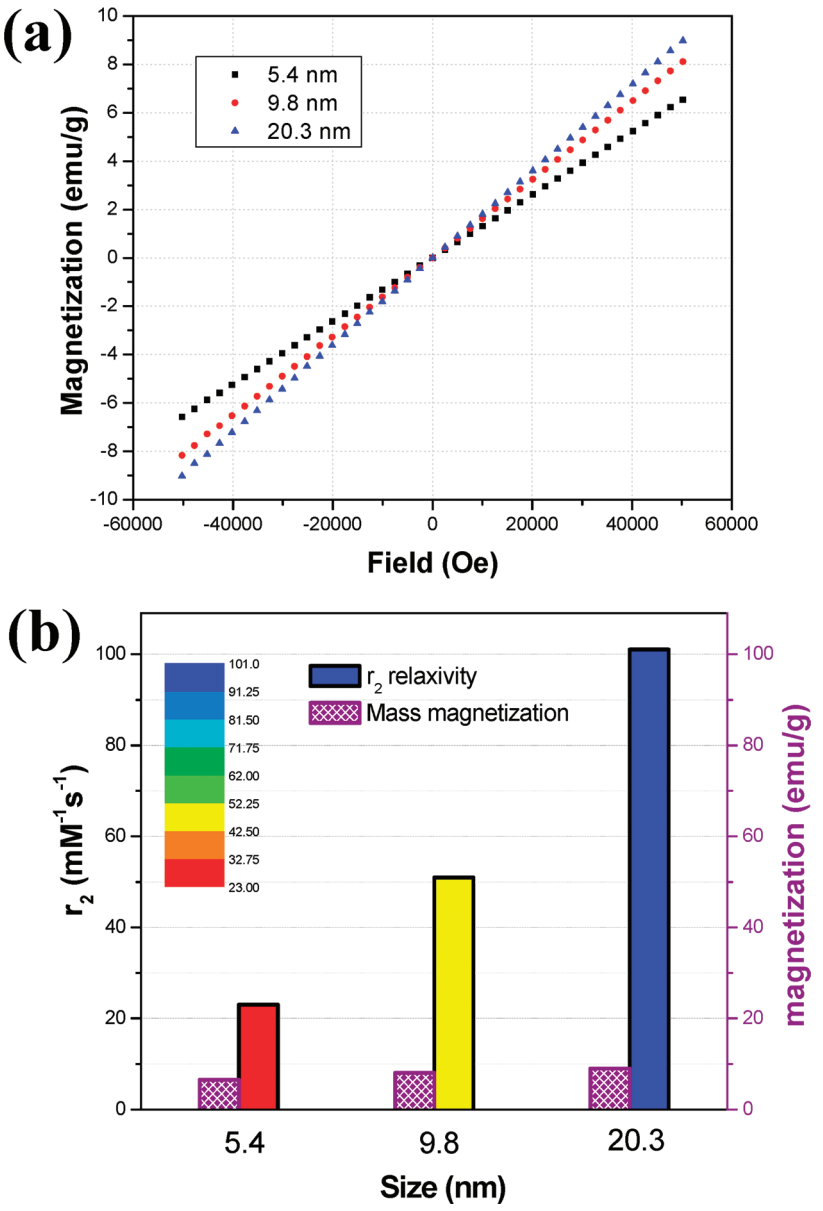

Figure 3. (a) Mass magnetization of the $NaDyF_4$ NPs obtained using a SQUID magnetometer. (b) Comparison of obtained r_2 relaxivity (at 9.4 T) of the three sizes of the NPs and corresponding mass magnetization (at 50 KOe).

discussed, contrast in T_2-weighted MR images is a consequence of high r_2 values, and the higher the r_2/r_1 ratio, the better the efficiency of the T_2 CA.[9,12] To compare the efficiency of the β-$NaDyF_4$ NPs, the r_2/r_1 ratios of the 20.3 nm β-$NaDyF_4$ NPs and the clinically used T_2 CAs such as Resovist, Feridex, and Combidex (r_2/r_1 = 31, 22.6, and 6, respectively, measured at 3 T)[33,34] are shown in Figure 2c. Figure 2c(iii) shows that the r_2/r_1 ratio of β-$NaDyF_4$ NPs is about 10 times higher than that of commercial CA Resovist at 9.4 T, which possesses the highest r_2 relaxivity. The r_2/r_1 ratio at 3 T is more than twice the commercial CAs. This extremely high r_2/r_1 of the β-$NaDyF_4$ NPs clearly suggests its high potential as T_2 CA at ultrahigh fields. In addition, it should also be noted that the r_2 relaxivity of a β-$NaDyF_4$ NP is much higher than that of Dy^{3+} chelates. For example, a 20.3 NP has a 474 times higher r_2 relaxivity than Dy complexes (e.g., Dy^{3+}-fullerenol), which substantiates the suitability of the materials and proves the advantage of using a NP-based contrast agent in terms of local contrast enhancement.

To demonstrate the consequence of higher relaxivity, T_2-weighted phantom MR images were obtained at 9.4 T. Figure 2c(ii) shows the images (at a 1.0 mM Dy^{3+} concentration) where the contrast of the image goes from gray to dark as the size gets bigger. The trend is a clear reflection of the obtained trend of mass magnetization and relaxivity of the NPs. The 20.3 nm NPs, which have shown an r_2 relaxivity of 101 $mM^{-1}\,s^{-1}$, were chosen for concentration-dependent (0.125−1.0 mM Dy^{3+}) phantom images to examine the feasibility of the NP for in vivo MR imaging. Figure 2c(iv) shows the concentration-dependent T_2-weighted phantom images of the water solutions of NPs, which show a clear concentration-dependent negative contrast gradient produced by the NPs. From the phantom MRI of the water solution of the NPs, it is evident that the 20.3 nm NPs can be used in T_2-weighted MR imaging to obtain contrast, which can easily be tuned by the concentration of the

dx.doi.org/10.1021/jz201664h | J. Phys. Chem. Lett. 2012, 3, 524–529

Table 2. Comparison of Dy^{3+}-based NPs and the Clinically Used T_2 CAs for MRI

contrast agents	surface coating	size[a] (nm)	HD[b] (nm)	r_2 (mM^{-1} s^{-1})	r_1 (mM^{-1} s^{-1})	r_2/r_1	field (T)	ref
$NaDyF_4$ NP	PMAO-PEG	20.3	33.7	101	0.33	306	9.4	this work
Dy^{3+}-based CAs								
Dy-fullerenol [$Dy@C_{82}(OH)_n$]				20			9.4	32
Dy-DTPA-PcHexPh$_2$				3	0.11	27	7	31
Dy_2O_3	D-glu. acid	2.9		40	0.16	250	3	18
Clinically Used CAs								
Combidex (Fe_3O_4)	dextran	5.85	35	60	10	6	1.5	34
Feridex (Fe_3O_4, γ-Fe_2O_3)	dextran	4.96	160	93	4.1	22	3	33
Resovist (Fe_3O_4)	carboxydextran	4	60	143	4.6	31	3	33

[a]Size based on TEM. [b]HD: hydrodynamic diameter based on DLS; D-glu. acid: D-glucuronic acid; DTPA-PcHexPh$_2$: 2-(R)-[(4,4-diphenylcyclohexyl)phosphonooxymethyl]-diethylenetriamine-*N,N,N′,N″N″*-pentaacetic acid.

NPs and their sizes. Table 2 shows a comparison of our Dy^{3+}-based NPs with the reported Dy^{3+}-based NPs and the clinically used T_2 CAs. Polydisperse and nonuniform Dy^{3+}-based NPs greater than 50 nm have not been compared to facilitate consistency in the comparison. The 20.3 nm β-$NaDyF_4$ NPs show much higher r_2 relaxivity with a very high r_2/r_1 value than the clinically used Combidex and Feridex CAs, which strongly suggests that these NPs could be excellent candidates as T_2 CAs for ultrahigh field MRI scanners. As compared in Table 2, the β-$NaDyF_4$ NPs are about the same size (HD) as the clinical agents, and the PEG chains impart biocompatibility. It is possible that different coatings to obtain biocompatibility (e.g., PEG and dextran) have subtle effects on the relaxivities, which warrants further systematic studies. Last, the relaxivity may be even more enhanced at higher field strengths, as demonstrated by Rosenberg et al.[11] at 21.1 T for Dy^{3+} complexes (in comparison to those at 9.4 T), because we have not yet reached saturation of the magnetization.

In conclusion, we have demonstrated that dysprosium-based NPs can be used as efficient T_2 contrast agents in ultrahigh field MRI using size-tunable β-$NaDyF_4$ NPs. The high r_2 relaxivity, extremely high r_2/r_1 ratio, and confirming MR phantom images suggest that the β-$NaDyF_4$ NPs are one of the strong candidates as T_2 CAs for the next generation of MRIs. Judicious modification of the NPs surface to modulate water exchange kinetics and achieve a longer rotational correlation time should lead to further optimization of the NPs relaxivity.

■ ASSOCIATED CONTENT

Supporting Information

Detailed experimental procedures, Figures S1–S3, and relaxivity equations. This material is available free of charge via the Internet at http://pubs.acs.org.

■ AUTHOR INFORMATION

Corresponding Author

*E-mail: fvv@uvic.ca. Tel: +1-250-721-7184. Fax: +1-250-721-7147.

Notes

The authors declare no competing financial interest.

■ ACKNOWLEDGMENTS

The authors are grateful to the Prostate Cancer Canada (Grant No. 2010-580) for the financial support of this work. Dr. Jody Spence (UVic) is acknowledged for ICP-MS analysis.

■ REFERENCES

(1) Blow, N. Functional Neuroscience: How to Get Ahead in Imaging. *Nature* **2009**, *458*, 925–928.

(2) Caravan, P. Strategies for Increasing the Sensitivity of Gadolinium Based MRI Contrast Agents. *Chem. Soc. Rev.* **2006**, *35*, 512–523.

(3) Garcia, J.; Neelavalli, J.; Haacke, E. M.; Allen, M. J. Eu^{II}-Containing Cryptates as Contrast Agents for Ultra-High Field Strength Magnetic Resonance Imaging. *Chem. Commun.* **2011**, *47*, 12858–12860.

(4) Tsutomu, N. Clinical Application of High and Ultra High-Field MRI. *Brain Dev.* **2007**, *29*, 325–335.

(5) Corot, C.; Robert, P.; Idée, J.-M.; Port, M. Recent Advances in Iron Oxide Nanocrystal Technology for Medical Imaging. *Adv. Drug Deliver. Rev.* **2006**, *58*, 1471–1504.

(6) Louie, A. Multimodality Imaging Probes: Design and Challenges. *Chem. Rev.* **2010**, *110*, 3146–3195.

(7) Na, H. B.; Song, I. C.; Hyeon, T. Inorganic Nanoparticles for MRI Contrast Agents. *Adv. Mater.* **2009**, *21*, 2133–2148.

(8) Gultepe, E.; Reynoso, F. J.; Jhaveri, A.; Kulkarni, P.; Nagesha, D.; Ferris, C.; Harisinghani, M.; Campbell, R. B.; Sridhar, S. Monitoring of Magnetic Targeting to Tumor Vasculature through MRI and Biodistribution. *Nanomedicine* **2010**, *5*, 1173–1182.

(9) Qin, J.; Laurent, S.; Jo, Y. S.; Roch, A.; Mikhaylova, M.; Bhujwalla, Z. M.; Muller, R. N.; Muhammed, M. A High-Performance Magnetic Resonance Imaging T_2 Contrast Agent. *Adv. Mater.* **2007**, *19*, 2411–2411.

(10) Helm, L. Optimization of Gadolinium-based MRI Contrast Agents for High Magnetic-Field Applications. *Future Med. Chem.* **2010**, *2*, 385–396.

(11) Rosenberg, J. T.; Kogot, J. M.; Lovingood, D. D.; Strouse, G. F.; Grant, S. C. Intracellular Bimodal Nanoparticles Based on Quantum Dots for High-Field MRI at 21.1 T. *Magn. Reson. Med.* **2010**, *64*, 871–882.

(12) Terreno, E.; Castelli, D. D.; Viale, A.; Aime, S. Challenges for Molecular Magnetic Resonance Imaging. *Chem. Rev.* **2010**, *110*, 3019–3042.

(13) Viswanathan, S.; Kovacs, Z.; Green, K. N.; Ratnakar, S. J.; Sherry, A. D. Alternatives to Gadolinium-Based Metal Chelates for Magnetic Resonance Imaging. *Chem. Rev.* **2010**, *110*, 2960–3018.

(14) Bulte, J. W. M.; Wu, C.; Brechbiel, M. W.; Brooks, R. A.; Vymazal, J.; Holla, M.; Frank, J. A. Dysprosium-DOTA-PAMAM Dendrimers as Macromolecular T_2 Contrast Agents: Preparation and Relaxometry. *Invest. Radiol.* **1998**, *33*, 841–845.

(15) Das, G. K.; Zhang, Y.; D'Silva, L.; Padmanabhan, P.; Heng, B. C.; Chye Loo, J. S.; Selvan, S. T.; Bhakoo, K. K.; Yang Tan, T. T. Single-Phase Dy_2O_3:Tb^{3+} Nanocrystals as Dual-Modal Contrast Agent for High Field Magnetic Resonance and Optical Imaging. *Chem. Mater.* **2011**, *23*, 2439–2446.

(16) Elst, L. V.; Roch, A.; Gillis, P.; Laurent, S.; Botteman, F.; Bulte, J. W. M.; Muller, R. N. Dy-DTPA Derivatives as Relaxation Agents for Very High Field MRI: The Beneficial Effect of Slow Water Exchange

on the Transverse Relaxivities. *Magn. Reson. Med.* **2002**, *47*, 1121−1130.
(17) Gossuin, Y.; Hocq, A.; Vuong, Q. L.; Disch, S.; Hermann, R. e. P.; Gillis, P. Physico-chemical and NMR Relaxometric Characterization of Gadolinium Hydroxide and Dysprosium Oxide Nanoparticles. *Nanotechnology* **2008**, *19*, 475102.
(18) Kattel, K.; Park, J. Y.; Xu, W.; Kim, H. G.; Lee, E. J.; Bony, B. A.; Heo, W. C.; Lee, J. J.; Jin, S.; Baeck, J. S. A Facile Synthesis, In Vitro and In Vivo MR Studies of D-Glucuronic Acid-Coated Ultrasmall Ln_2O_3 (Ln = Eu, Gd, Dy, Ho, and Er) Nanoparticles as a New Potential MRI Contrast Agent. *ACS Appl. Mater. Interfaces* **2011**, *3*, 3325−3334.
(19) Norek, M.; Peters, J. A. MRI Contrast Agents Based on Dysprosium or Holmium. *Prog. Nucl. Magn. Reson. Spectrosc.* **2011**, *59*, 64−82.
(20) Norek, M. g.; Kampert, E.; Zeitler, U.; Peters, J. A. Tuning of the Size of Dy_2O_3 Nanoparticles for Optimal Performance as an MRI Contrast Agent. *J. Am. Chem. Soc.* **2008**, *130*, 5335−5340.
(21) Ho, D.; Sun, X.; Sun, S. Monodisperse Magnetic Nanoparticles for Theranostic Applications. *Acc. Chem. Res.* **2011**, *44*, 875−882.
(22) Johnson, N. J. J.; Oakden, W.; Stanisz, G. J.; Scott Prosser, R.; van Veggel, F. C. J. M. Size-Tunable, Ultrasmall $NaGdF_4$ Nanoparticles: Insights into Their T_1 MRI Contrast Enhancement. *Chem. Mater.* **2011**, *23*, 3714−3722.
(23) Vetrone, F.; Naccache, R.; Morgan, C. G.; Capobianco, J. A. Luminescence Resonance Energy Transfer from an Upconverting Nanoparticle to a Fluorescent Phycobiliprotein. *Nanoscale* **2010**, *2*, 1185−1189.
(24) Wang, F.; Banerjee, D.; Liu, Y.; Chen, X.; Liu, X. Upconversion Nanoparticles in Biological Labeling, Imaging, and Therapy. *Analyst* **2010**, *135*, 1839−1854.
(25) Zhang, J.; Shade, C. M.; Chengelis, D. A.; Petoud, S. A Strategy to Protect and Sensitize Near-infrared Luminescent Nd^{3+} and Yb^{3+}: Organic Tropolonate Ligands for the Sensitization of Ln^{3+}-Doped $NaYF_4$ Nanocrystals. *J. Am. Chem. Soc.* **2007**, *129*, 14834−14835.
(26) Hou, Z. Y.; Li, C. X.; Ma, P. A.; Li, G. G.; Cheng, Z. Y.; Peng, C.; Yang, D. M.; Yang, P. P.; Lin, J. Electrospinning Preparation and Drug-Delivery Properties of an Up-conversion Luminescent Porous $NaYF_4$:Yb^{3+}, Er^{3+}@Silica Fiber Nanocomposite. *Adv. Funct. Mater.* **2011**, *21*, 2356−2365.
(27) Zhang, F.; Shi, Q. H.; Zhang, Y. C.; Shi, Y. F.; Ding, K. L.; Zhao, D. Y.; Stucky, G. D. Fluorescence Upconversion Microbarcodes for Multiplexed Biological Detection: Nucleic Acid Encoding. *Adv. Mater.* **2011**, *23*, 3775−3779.
(28) Wang, G. F.; Peng, Q.; Li, Y. D. Lanthanide-Doped Nanocrystals: Synthesis, Optical−Magnetic Properties, and Applications. *Acc. Chem. Res.* **2011**, *44*, 322−332.
(29) Zhou, J.; Yu, M. X.; Sun, Y.; Zhang, X. Z.; Zhu, X. J.; Wu, Z. H.; Wu, D. M.; Li, F. Y. Fluorine-18-Labeled Gd^{3+}/Yb^{3+}/Er^{3+} Co-doped $NaYF_4$ Nanophosphors for Multimodality PET/MR/UCL Imaging. *Biomaterials* **2011**, *32*, 1148−1156.
(30) Jun, Y.-W.; Lee, J.-H.; Cheon, J. Chemical Design of Nanoparticle Probes for High-Performance Magnetic Resonance Imaging. *Angew. Chem., Int. Ed.* **2008**, *47*, 5122−5135.
(31) Caravan, P.; Greenfield, M. T.; Bulte, J. W. M. Molecular Factors that Determine Curie Spin Relaxation in Dysprosium Complexes. *Magn. Reson. Med.* **2001**, *46*, 917−922.
(32) Kato, H.; Kanazawa, Y.; Okumura, M.; Taninaka, A.; Yokawa, T.; Shinohara, H. Lanthanoid Endohedral Metallofullerenols for MRI Contrast Agents. *J. Am. Chem. Soc.* **2003**, *125*, 4391−4397.
(33) Rohrer, M.; Bauer, H.; Mintorovitch, J.; Requardt, M.; Weinmann, H.-J. Comparison of Magnetic Properties of MRI Contrast Media Solutions at Different Magnetic Field Strengths. *Invest. Radiol.* **2005**, *40*, 715−724.
(34) Wang, Y.-X. J. Superparamagnetic Iron Oxide Based MRI Contrast Agents: Current Status of Clinical Application. *Quant. Imaging Med. Surg.* **2011**, *1*, 35−40.